

# Tailoring Crystallization Kinetics of Chalcogenides for Photonic Applications

Maximilian J. Müller, Aakash Yadav, Christoph Persch, Sophia Wahl, Felix Hoff, and Matthias Wuttig\*

Chalcogenides possess interesting optical properties, which are attractive for a variety of applications such as data storage, neuromorphic computing, and photonic switches. Lately a group of covalently bonded chalcogenides including  $\text{Sb}_2\text{Se}_3$  and  $\text{Sb}_2\text{S}_3$  has moved into the focus of interest for such photonic applications, where high optical contrast as well as reliable and fast switching is of crucial importance. Here, these properties of  $\text{Sb}_2\text{Se}_3$  are examined and compared with typical phase change materials such as  $\text{GeSb}_2\text{Te}_4$  and  $\text{Ge}_2\text{Sb}_2\text{Te}_5$ .  $\text{Sb}_2\text{Se}_3$  is favorable for many photonic applications due to its larger band gap, yet, the maximum optical contrast achievable is smaller than for  $\text{GeTe}$  and  $\text{Ge}_2\text{Sb}_2\text{Te}_5$ . Furthermore, crystallization needs significantly longer and exhibits a distinctively wider stochastic distribution of reflectances after crystallization, which provides challenges for the usage in photonic applications. At the same time, the glassy/amorphous state of  $\text{Sb}_2\text{Se}_3$  is more stable. These differences can be attributed to differences in bonding of the crystalline state, which is more covalent for  $\text{Sb}_2\text{Se}_3$ . A quantum-chemical map can help to understand and explain these trends and facilitates the design of tailored materials for photonic applications.

materials can be rapidly and reversibly switched between two different solid phases, usually an amorphous and a crystalline state. This phase transition is accompanied by pronounced changes of optical and electrical properties. The combination of pronounced property changes and the ability to switch rapidly makes these materials attractive for a number of applications ranging from rewritable optical data storage<sup>[4–6]</sup> to non-volatile electronic memories,<sup>[7,8]</sup> photonic switches,<sup>[9,10]</sup> and neuromorphic computing.<sup>[11,12]</sup> The corresponding class of materials are designated as phase change materials. Please note that there is another class of materials, often based on paraffin waxes, which are also denoted as phase change materials. Yet, these materials are characterized by a considerable latent heat release upon crystallization, a property which makes them attractive for thermal energy storage and release. In this paper,

we will only deal with phase change materials for information storage and processing.

To understand the full prospect of chalcogenides in these different applications and hence explore the potential of these emerging technologies, it is highly desirable to understand the range of property changes that can be realized with these chalcogenides and to know the speed limits of the switching process<sup>[13–15]</sup> and the minimum power consumption that can be realized.<sup>[16]</sup> It would be particularly helpful, if a clear understanding of the stoichiometry dependence of property changes and switching speed could be obtained for phase change materials. This information could provide clear guidelines for the optimization and design potential of these chalcogenides.

To reach this goal, it is very helpful if changes in stoichiometry can be quantified. Recently a scheme has been suggested which characterizes the chemical bond between adjacent atoms by the number of electrons shared and transferred between these atoms.<sup>[17]</sup> With this map, solids could be separated which use different bonding mechanisms such as metallic, ionic, or covalent bonding. Interestingly, chalcogenides such as  $\text{GeTe}$ ,  $\text{PbTe}$ ,  $\text{AgSbTe}_2$ , or  $\text{Sb}_2\text{Te}_3$  are all located in a unique region of the map, characterized by small electron transfer and sharing of about one electron between two adjacent atoms.<sup>[18]</sup>

With a single electron shared between these two atoms, this bond differs clearly from covalent bonding, where an electron pair holds two atoms together. Yet, the bond in these


## 1. Introduction

Chalcogenides such as  $\text{GeTe}$ ,  $\text{Ge}_2\text{Sb}_2\text{Te}_5$ , or  $\text{Sb}_2\text{Te}_3$  doped with Ag and In (AIST) are frequently used to store data.<sup>[1–3]</sup> These

M. J. Müller, A. Yadav, C. Persch, S. Wahl, F. Hoff, M. Wuttig  
 Institute of Physics  
 Physics of Novel Materials  
 RWTH Aachen University  
 52056 Aachen, Germany  
 E-mail: wuttig@physik.rwth-aachen.de

M. Wuttig  
 Jülich-Aachen Research Alliance (JARA FIT and JARA HPC)  
 RWTH Aachen University  
 52056 Aachen, Germany

M. Wuttig  
 PGI 10 (Green IT)  
 Forschungszentrum Jülich GmbH  
 52428 Jülich, Germany

 The ORCID identification number(s) for the author(s) of this article can be found under <https://doi.org/10.1002/aelm.202100974>.

© 2021 The Authors. Advanced Electronic Materials published by Wiley-VCH GmbH. This is an open access article under the terms of the Creative Commons Attribution-NonCommercial License, which permits use, distribution and reproduction in any medium, provided the original work is properly cited and is not used for commercial purposes.

DOI: 10.1002/aelm.202100974

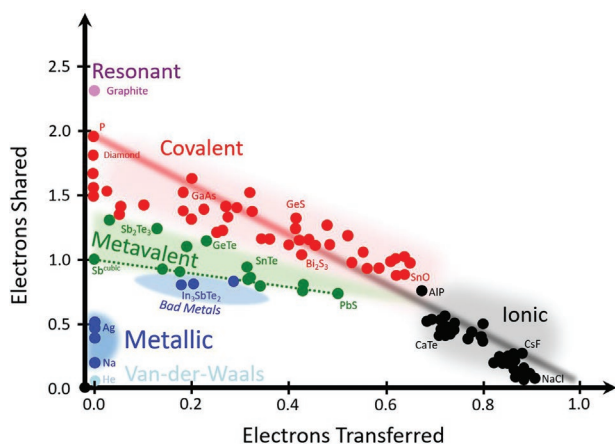


**Figure 1.** Map of materials spanned by two coordinates, the number of electrons transferred and shared between adjacent atoms. The number of electrons transferred is normalized by the oxidation state of the element. Different materials employing covalent, ionic and metallic bonding cluster in different areas of the map, marked by color. Typical phase change materials such as  $\text{Sb}_2\text{Te}_3$  and  $\text{GeTe}$  cluster in a well-defined region between covalent and metallic systems. They are characterized by unconventional properties, indicative for a distinct bonding mechanism denoted as metavalent bonding. Reproduced with permission.<sup>[21]</sup> Copyright 2021, Wiley-VCH.

chalcogenides is also not predominantly ionic, since the charge transfer is quite small. The unique property portfolio of these chalcogenides,<sup>[19]</sup> their unconventional bond rupture,<sup>[20]</sup> the special region they occupy in the map depicted in **Figure 1**, as well as the discontinuous property changes upon the transition to covalent bonding<sup>[21]</sup> provide clear evidence that these materials employ an unconventional bonding mechanism, which differs from metallic, ionic, and covalent bonding. This bonding mechanism has been denoted as “metavalent bonding.” Materials such as the chalcogenides mentioned above use this bonding mechanism, which is characterized by a competition between electron localization as in covalent (or ionic) bonding and electron delocalization as in metallic bonding.

Further insights are obtained, if the orbital view of chemistry is combined with the band structure perspective of physics. The relevant orbitals that form the bond in  $\text{GeTe}$ ,  $\text{PbTe}$ , or  $\text{Sb}_2\text{Te}_3$  are the p-orbitals of adjacent atoms. Overlapping p-orbitals form a  $\sigma$ -bond between adjacent atoms in these solids, which employ an octahedral-like atomic arrangement. This  $\sigma$ -bond is only filled by a single electron, giving rise to a half-filled band, which should lead to a metallic state. Yet, moderate charge transfers or a slight atomic rearrangement (often discussed in the framework of “Peierls distortions”), opens up a small band gap. Therefore, these materials are also denoted as “incipient metals.”

Since the states both above and below the Fermi level are due to p-electrons, the optical properties are also governed by transitions between p-states. These transitions are allowed by the dipole selection rule, since the parity of the states changes upon the transition. The strength of the optical transition and hence the maximum of the imaginary part of the dielectric function  $\epsilon_2(\omega)$  decreases with increasing charge transfer (ET) between adjacent atoms<sup>[22]</sup> and/or with increasing Peierls distortion, which leads to an increase of the number of electrons shared between adjacent atoms. Both increasing charge transfer or

an increase of ES lead to a reduction in the overlap between occupied and empty states below and above the Fermi energy, respectively; causing a reduction of the maximum of  $\epsilon_2(\omega)$ .

Hence, the most pronounced absorption is found for those crystalline chalcogenides which are located in the lower left corner of the metavalent (green) region of **Figure 1**. Amorphous phase change materials, on the contrary, are characterized by a more pronounced Peierls distortion<sup>[23]</sup> and hence a smaller optical absorption and a larger band gap. This explains the optical contrast between the amorphous and crystalline state in  $\text{GeTe}$  or  $\text{Sb}_2\text{Te}_3$ .<sup>[24]</sup>

Yet, the map in **Figure 1** has even more predictive and explanatory power. Going from the lower left corner in the metavalently bonded region toward materials with more Peierls distortion decreases the optical contrast and reduces the crystallization speed, since the bonds are getting stronger.<sup>[25]</sup> This leads apparently to an increase of the activation barrier for crystallization. It also increases the ease of glass formation and hence the stability of the amorphous, i.e., glassy state characterized by  $T_{ro}$ , the reduced onset temperature of glass transition, from 0.47 ( $\text{GeTe}$ ) to 0.58 ( $\text{GeSe}$ ).<sup>[25]</sup>

The key challenge for metavalently bonded materials is thus the realization of pronounced optical contrast for photon energies of 1 eV and above, to enable a significant optical response in the visible range. Since the crystalline chalcogenides in the green region of **Figure 1** all have rather small band gaps, typically below 1 eV, it is difficult to realize photonic switches, which can also be employed in this range. Hence, in the last decade numerous attempts have been undertaken to identify phase change materials with larger band gap. Replacing Te by Se has been one approach followed by several groups.<sup>[26,27]</sup> In recent years, even sulfides have been explored. The most interesting suggestion has been the exploration of  $\text{Sb}_2\text{Se}_3$  and  $\text{Sb}_2\text{S}_3$  for photonic applications.<sup>[28,29]</sup> These two sesqui-chalcogenides have band gaps of 1.16<sup>[30]</sup> and 1.7 eV,<sup>[31]</sup> respectively and hence can be used at higher photon energies.

## 2. Results and Discussion

### 2.1. Optical Contrast

For typical glasses of covalent network formers, the short range order is very similar in the amorphous and the crystalline state. This was first claimed by Zachariassen in 1932.<sup>[32]</sup> Glasses which follow his rule are thus sometimes denoted as Zachariassen glasses. For such materials, the optical contrast between the two phases is attributed to a density contrast between the two phases as explained in the Clausius–Mossotti relation, which relates the index of refraction of a solid to its density. A sufficient density change upon crystallization will thus lead to a noticeable change of the refractive index. Since the density change upon crystallization is typically 5% or less,<sup>[33]</sup> the resulting change in refractive index is typically quite modest. Much larger changes of optical properties, and in particular the refractive index are observed upon crystallization of most phase change materials, where the refractive index can increase by 50% and more. This pronounced change has been attributed to a change in bonding upon crystallization.<sup>[24,34]</sup> At first, the bonding in crystalline phase change materials had been denoted as resonant bonding,

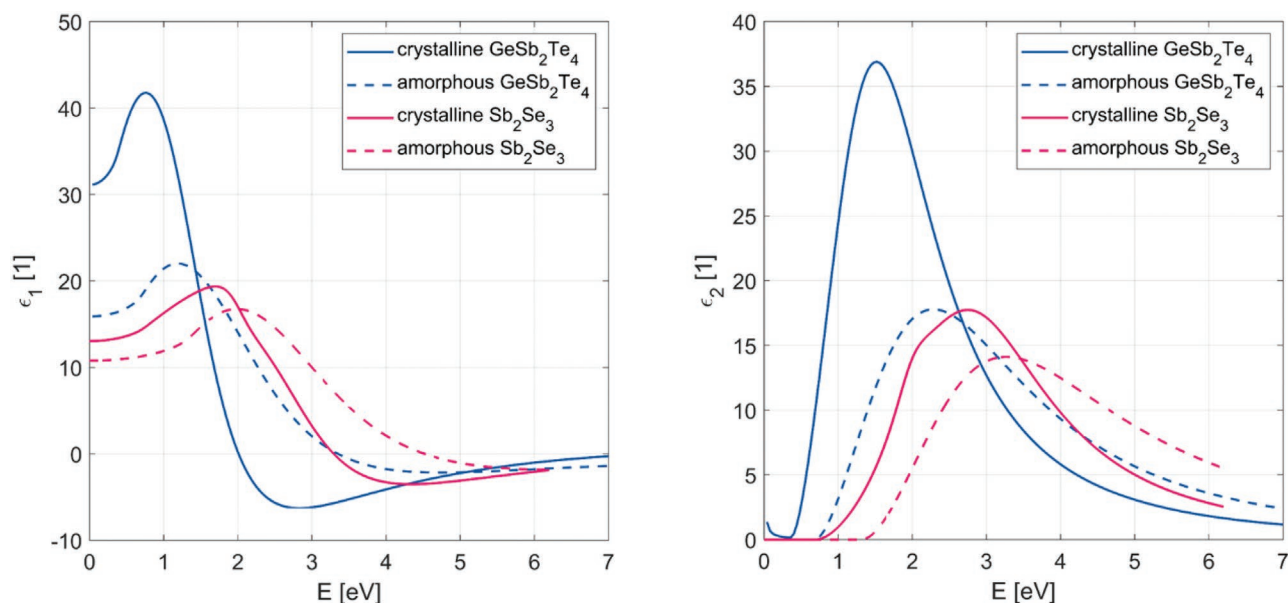


**Figure 2.** Comparison of the dielectric function for the crystalline and amorphous phase between a typical phase change material ( $\text{GeSb}_2\text{Te}_4$ ) and a covalently bonded system ( $\text{Sb}_2\text{Se}_3$ ). The real and imaginary part of the dielectric function are shown on the right and left side, respectively. The optical contrast is more pronounced for  $\text{GeSb}_2\text{Te}_4$ . For  $\text{Sb}_2\text{Se}_3$ , the larger band gap shifts the absorption maximum to higher energies.

a bonding mechanism introduced by Linus Pauling to explain the unconventional properties of benzene. Later, however, it has been shown that the bonding in benzene or graphite differs significantly from the bonding in phase change materials such as  $\text{GeTe}$  and  $\text{Sb}_2\text{Te}_3$ . A few years ago, the bonding in crystalline phase change materials has been denoted as metavalent bonding for reasons explained in the introduction. On the contrary, in the amorphous phase covalent bonding is employed.<sup>[5]</sup> This change in bonding enables a much larger optical contrast upon crystallization as depicted in **Figure 2**. This has been explained in a number of recent studies which focus on the change in the local atomic arrangement and its consequences on the optical properties. The crystalline phase is characterized by a modest Peierls distortion, while the amorphous phase presumably features a significantly larger distortion and hence smaller absorption.<sup>[21,24,35]</sup>

## 2.2. Switching Kinetics

For photonic applications, reliable optical switching (i.e., crystallization) is indispensable. **Figure 3** compares the typical phase change material  $\text{Ge}_2\text{Sb}_2\text{Te}_5$  with  $\text{Sb}_2\text{Se}_3$ , a novel material suggested recently to enable switching at shorter laser wavelengths. Both materials can be crystallized for a wide range of laser powers between 10 and 50 mW. However, the crystallization processes of the two materials differ dramatically in terms of speed and the stochastics of the reflectance in the crystalline phase. While  $\text{Ge}_2\text{Sb}_2\text{Te}_5$  can be crystallized within  $10^2$  ns, the same process takes more than  $3 \times 10^5$  ns for  $\text{Sb}_2\text{Se}_3$ . This material is thus much slower than the typical phase change material  $\text{Ge}_2\text{Sb}_2\text{Te}_5$ . Equally important, while for  $\text{Ge}_2\text{Sb}_2\text{Te}_5$  the reflectance change upon crystallization is very reproducible, i.e., depends only upon pulse length and pulse power, a distinct

scattering can be observed for  $\text{Sb}_2\text{Se}_3$ , ranging from 5% to 25% reflectance change during crystallization. This can be seen if we average the reflectivity contrast over the closest 2 pulses in any direction. For  $\text{Ge}_2\text{Sb}_2\text{Te}_5$ , this does hardly change the PTE diagram, while a drastic reduction in reflectivity change amplitude is observed for  $\text{Sb}_2\text{Se}_3$ . For storage and switching applications this scattering is highly disadvantageous since it would severely hinder a reliable storage of information and impedes the realization of a multilevel memory or switch.

Since crystallization of  $\text{Sb}_2\text{Se}_3$ , which is covalently bonded, is rather slow, compared to typical phase change materials such as  $\text{Sb}_2\text{Te}_3$  and  $\text{GeTe}$ ,<sup>[13–15]</sup> which are metavalently bonded, one can ponder if alloys of  $\text{Sb}_2\text{Se}_3$  can be found, which still have a significant contrast of optical properties at short laser wavelengths, yet enable faster switching speeds. The minimum crystallization time of  $\text{Sb}_2\text{Se}_{3x}\text{Te}_{3(1-x)}$ -alloys was determined with this goal in mind. Only stoichiometries of  $x = 0.4$  and above can be studied with PTE diagrams as shown in **Figure 3**. The  $\text{Sb}_2\text{Te}_3$  rich alloys are already partly crystalline as deposited due to their low crystallization temperature.  $\text{Sb}_2\text{Se}_3$  rich alloys, with  $x$  above 0.6 cannot be used either, because they exhibit a miscibility gap, and crystallization would be dominated by the crystallization of the fastest component. The results of those alloys that can be crystallized and form a single crystalline phase are presented in **Figure 4**. The probability of nucleation was determined by examining at which probability a significant contrast change caused by crystal nucleation can be detected for a given pulse length. Further explanations of this calculation can be found in the Section S1 (Supporting Information). The minimum crystallization time of  $\text{Sb}_2\text{Se}_{3x}\text{Te}_{3(1-x)}$ -alloys, depicted as a vertical line, increases by more than two orders of magnitude by moving from  $x = 0.4$ –0.6. The minimum crystallization time increases further to  $\tau = 3.1 \times 10^5$  ns for  $\text{Sb}_2\text{Se}_3$ . This trend is in excellent agreement with a trend found earlier for compounds

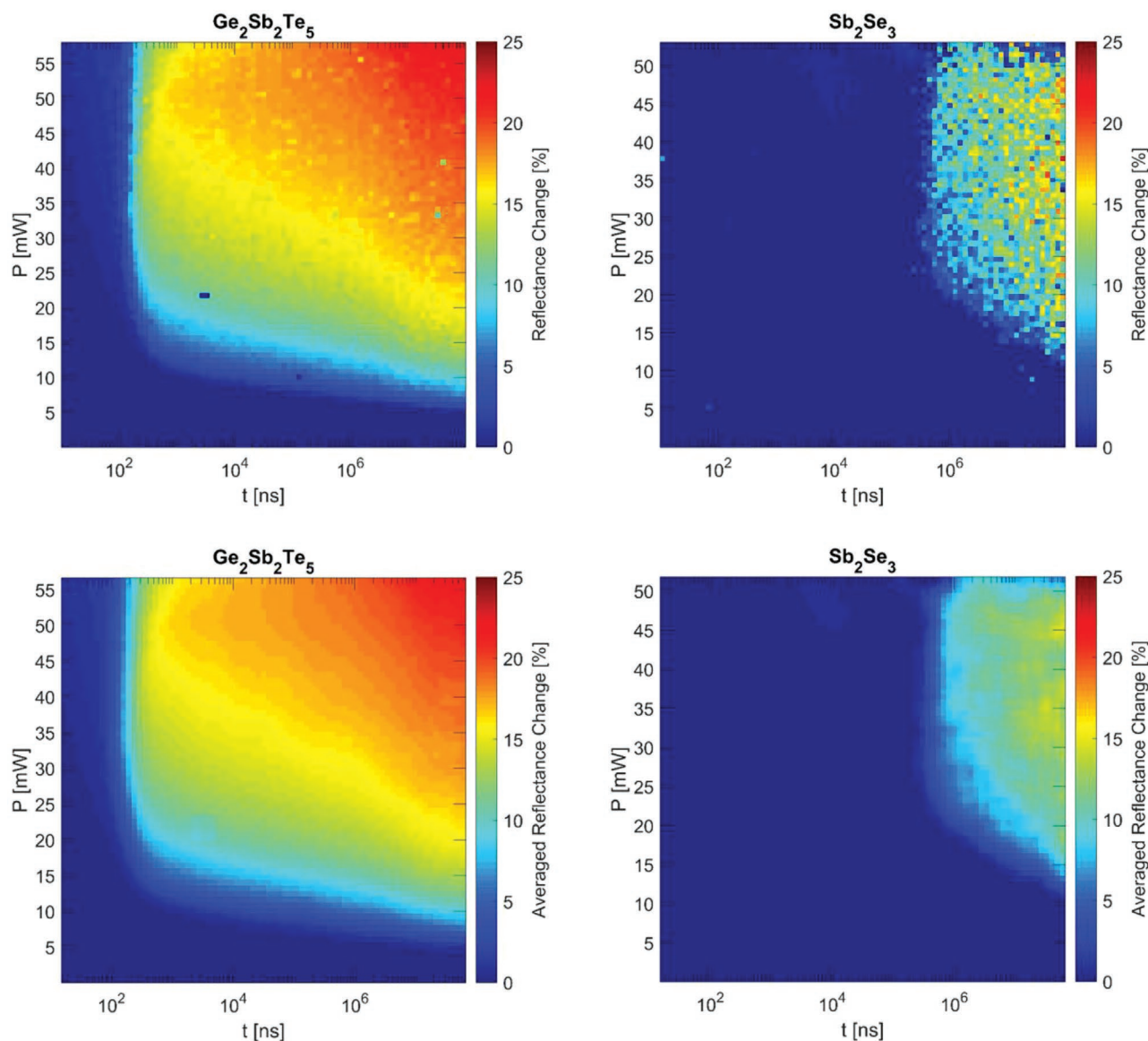


**Figure 3.** Power–Time–Effect diagrams (PTE) for an optical crystallization experiment of a typical phase change material ( $\text{Ge}_2\text{Sb}_2\text{Te}_5$ ) and of a covalently bonded material ( $\text{Sb}_2\text{Se}_3$ ) in the upper graphs. Both materials show crystallization for a wide range of laser pulse powers. For both materials, the pulse length needed for crystallization to start becomes independent of laser pulse powers above 20 mW. The reflectance change upon crystallization is much more stochastic for  $\text{Sb}_2\text{Se}_3$  than for  $\text{Ge}_2\text{Sb}_2\text{Te}_5$ . In the lower graphs the reflectance change is averaged over two points in each direction. It can clearly be seen that  $\text{Ge}_2\text{Sb}_2\text{Te}_5$  in contrast to  $\text{Sb}_2\text{Se}_3$  barely changes due to averaging and has a distinctly larger average contrast.

such as GeTe or SnTe, which crystallized systematically faster than covalent bonded compounds such as GeSe.<sup>[25]</sup>

This stoichiometry dependence can even be presented more quantitatively by using the quantum mechanical map of bonding introduced above. For this purpose, the coordinates of this map, the electrons shared and electrons transferred, are calculated as described in.<sup>[17]</sup> It has been found that the crystallization time increases with an increasing number of electrons shared between adjacent atoms. **Figure 5** shows that  $\text{Sb}_2\text{Se}_3$  follows this trend. This indicates that the number of electrons shared in the crystalline state of a given phase change material is an indicator of its crystallization kinetics both for metalloid bonded materials such as GeTe,  $\text{Sb}_2\text{Te}_3$ , and their alloys

and covalently bonded systems such as  $\text{Sb}_2\text{Se}_3$ , and presumably also  $\text{Sb}_2\text{S}_3$ . It hence remains a large challenge to identify photonic switches with short operation wavelength that can be rapidly switched.

We have refrained from plotting the mixed  $\text{Sb}_2\text{Se}_{3-x}\text{Te}_{3(1-x)}$ -alloys around  $x = 0.5$  in **Figure 5**, because there is no reliable way to compute the bonding quantifier ES and ET for arbitrary three-compound-materials, as long as the details of the atomic arrangement of the atoms, such as the size of their Peierls distortion is not known precisely. In the future, it would be highly advantageous to find a method to include such compounds into the map in a systematic manner to increase its predictive power also for more complicated compounds.

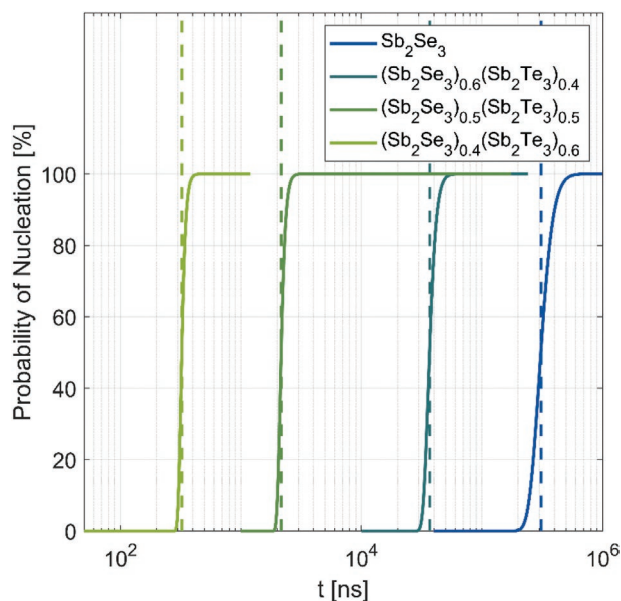


**Figure 4.** Probability of nucleation as a function of pulse length in an optical switching experiment. The minimum crystallization time  $\tau$  is defined as the time where the probability of nucleation equals 50%, denoted with a vertical line. A clear trend of an increase of nucleation time  $\tau$  with Se content is observed. Further explanations on how to determine  $\tau$  can be found in the Section S1 (Supporting Information).

### 2.3. Vitrification

Besides the crystallization kinetics, vitrification kinetics is also important, since it is necessary to ensure the stability of the amorphous state, i.e., ensure its nonvolatility. Vitrification kinetics predicts if this can be realized for a given material. Numerous studies have tried to identify systematic trends in the vitrification of chalcogenides, as shown.<sup>[36,37]</sup> For this purpose, the onset temperature of glass transition  $T_0$  is frequently determined using differential scanning calorimetric (DSC)

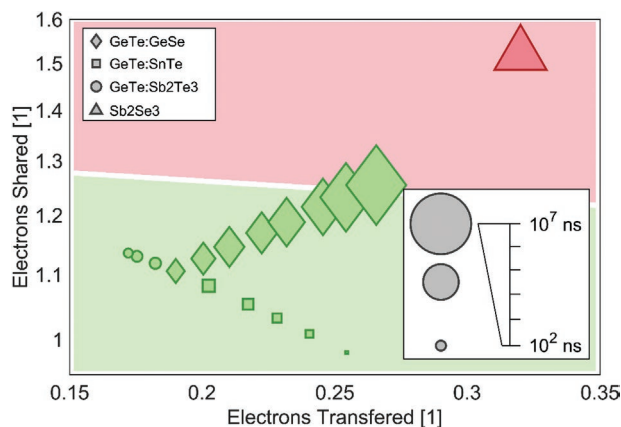


**Figure 5.** Minimum crystallization time  $\tau$  and its dependence on the chemical bond indicators introduced in Figure 1.  $\text{Sb}_2\text{Se}_3$  represents a covalently bonded material, while typical phase change materials such as  $\text{Ge}_2\text{Sb}_2\text{Te}_5$  or  $\text{GeTe}$  are metavalently bonded. Data for other compounds than  $\text{Sb}_2\text{Se}_3$  is taken.<sup>[25]</sup>

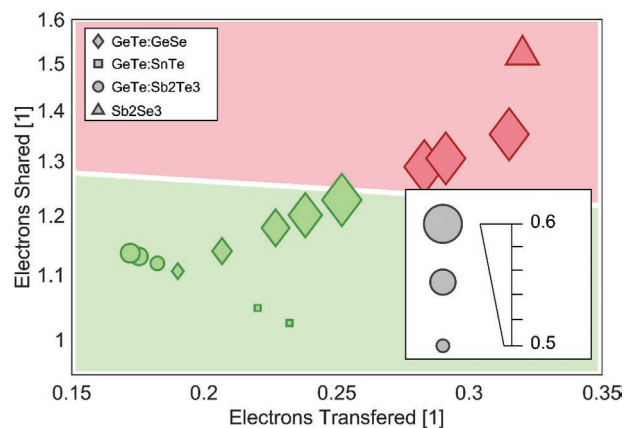


**Figure 6.** Reduced onset temperature of glass transition  $T_0$  and its dependence on the chemical bond indicators introduced in Figure 1.  $\text{Sb}_2\text{Se}_3$  represents a covalently bonded material, while typical phase change materials such as  $\text{Ge}_2\text{Sb}_2\text{Te}_5$  or  $\text{GeTe}$  are metavalently bonded. Data for other compounds than  $\text{Sb}_2\text{Se}_3$  is taken.<sup>[25]</sup>

measurements. Since  $T_0$  depends upon the absolute bond strength and is thus hard to compare for different systems,  $T_0$  is usually divided by the melting temperature  $T_m$  to determine the reduced onset temperature of glass transition  $T_{r0} = T_0/T_m$ . Because the standard glass transition is hard to detect in typical phase change materials such as  $\text{GeTe}$ ,<sup>[38,39]</sup>  $T_0$  was determined for all materials at a high heating rate of  $6 \times 10^4 \text{ K min}^{-1}$ . An explanation of the specific methodology to determine  $T_{r0}$  can be found in the Section S2 (Supporting Information). Like  $\tau$  the reduced onset temperature of the glass transition  $T_{r0}$  seems to follow the previously observed trend of being higher for compounds with higher numbers of electrons shared, i.e., more covalently bonded compounds, which is shown in Figure 6.<sup>[25]</sup>

## 3. Conclusion

Systematic trends for the crystallization and vitrification kinetics as well as the optical contrast as a function of chemical bond indicators are depicted. These trends show that metavalently bonded materials reveal large changes of optical properties upon crystallization and high switching speeds. Crystallization becomes increasingly sluggish and the contrast decreases upon bond stiffening, e.g. upon increasing the number of electrons shared between adjacent atoms. The contrast between the amorphous and crystalline phase for  $\text{Sb}_2\text{Se}_3$ , which is covalently bonded, is small compared to the contrast of a typical phase change material, since the optical contrast in  $\text{Sb}_2\text{Se}_3$  is merely a result of the density contrast between both phases. Furthermore, the change in optical properties upon crystallization is much more stochastic, creating difficulties for reproducible switches and multilevel memories.

## 4. Experimental Section

**Sample Preparation:** Thin film samples of  $\text{Sb}_2\text{Se}_3$  and  $\text{GeSb}_2\text{Te}_4$  for optical and switching measurements are prepared via sputter deposition from stoichiometric targets. Samples of the pseudo binary line of

$\text{Sb}_2\text{Se}_3\text{Te}_{3(1-x)}$  were co-sputtered using a  $\text{Sb}_2\text{Se}_3$  and a  $\text{Sb}_2\text{Te}_3$  target. The substrates are rotating over the targets with a sufficiently high rotation speed that layer by layer growth of the two source materials is prevented. As substrate Si (100) was used. The optical samples have a thickness of 500 nm and are capped with a layer of 5 nm thick  $(\text{ZnS})_{80}(\text{SiO}_2)_{20}$  to prevent them from oxidation. The switching samples have a thickness of 30 nm and are capped with a layer of 100 nm thick  $(\text{ZnS})_{80}(\text{SiO}_2)_{20}$ . Additionally, a layer of 10 nm thick  $(\text{ZnS})_{80}(\text{SiO}_2)_{20}$  is deposited below the phase change layer as heat barrier to increase the temperature during the laser pulse. The amorphous phase of the as deposited samples was verified with x-ray diffraction measurements. Powder samples for calorimetric measurements were also sputtered from a stoichiometric  $\text{Sb}_2\text{Se}_3$  target as a layer of thickness 6  $\mu\text{m}$ . The material was exfoliated and carefully stirred to powder afterwards.

**Optical Investigation:** For the optical investigation of  $\text{Sb}_2\text{Se}_3$  films, ellipsometry spectra have been measured in the range from 5900 to 41 000  $\text{cm}^{-1}$  using a J.A. Woolam M-2000UI. The data was collected at angles of incidence of 65°, 70°, and 75° at room temperature and then analyzed using the software Code by W. Theiss and the dielectric function was extrapolated accordingly.

**Switching Experiment:** The crystallization experiments were performed with an optical pump probe setup. The switching is performed with a rectangular laser pulse of a wavelength of 658 nm. The pulse length can be freely modified between 10<sup>1</sup> and 10<sup>8</sup> ns by using an arbitrary wave generator. In addition, the pulse power can be adjusted between 0 and 90 mW, which corresponds to a power density up to  $4.3 \times 10^6 \text{ W cm}^{-2}$ . During the experiment the sample's reflectance is continuously probed with a 639 nm wavelength laser at low power of 50  $\mu\text{W}$ . By changing the pulse parameters, a Power–Time–Effect (PTE-diagram) can be obtained to visualize the complete switching kinetics of a sample.

**Calorimetric Measurements:** Calorimetric measurements were performed with a Flash DSC 1 from Mettler Toledo (FDSC). The measurements were performed with a single particle of powder placed directly on the sensor of the FDSC. This way very high heating rates can be achieved. The measurement protocol consists of two identical, consecutive heating runs with a constant heating rate of  $6 \times 10^4 \text{ K min}^{-1}$ . In the first run the amorphous powder particle crystallizes. The second run, in which the particle is crystalline from the start, is subtracted from the first run. On this way the measurement is calibrated to the heat capacity of the crystalline phase. The measurements were repeated 10 times that the determined onset temperature can be averaged. The used sensor was calibrated with the melting temperature of Indium after the measurements were performed.

## Supporting Information

Supporting Information is available from the Wiley Online Library or from the author.

## Acknowledgements

This work was supported in part by the Deutsche Forschungsgemeinschaft (SFB 917) and in part by the Federal Ministry of Education and Research (BMBF, Germany) in the project NEUROTEC (16ES1133 K), M.W. furthermore acknowledges funding of a Distinguished Professorship by RWTH Aachen University. The authors also acknowledge the work of Yudong Cheng who helped with measuring the dielectric function of  $\text{GeSb}_2\text{Te}_4$ , Oliver Krause who helped preparing the  $\text{Ge}_2\text{Sb}_2\text{Te}_5$  sample and Sebastian Gruner as well as Stephan Gräbe for conducting the x-ray diffraction measurements.

Open access funding enabled and organized by Projekt DEAL.

## Conflict of Interest

The authors declare no conflict of interest.

## Data Availability Statement

Research data are not shared.

## Keywords

crystal growth, crystallization kinetics, materials design, metavalent bonding, nucleation, photonic applications, vitrification

Received: September 10, 2021

Revised: October 8, 2021

Published online: November 21, 2021

- [1] M. Chen, K. A. Rubin, R. Barton, *Appl. Phys. Lett.* **1986**, 49, 502.
- [2] P. Fantini, *J. Phys. D: Appl. Phys.* **2020**, 53, 283002.
- [3] S. W. Fong, C. M. Neumann, H.-S. P. Wong, *IEEE Trans. Electron Devices* **2017**, 64, 4374.
- [4] M. Wuttig, N. Yamada, *Nat. Mater.* **2007**, 6, 824.
- [5] B. J. Kooi, M. Wuttig, *Adv. Mater.* **2020**, 32, 1908302.
- [6] W. Zhang, R. Mazzarello, M. Wuttig, E. Ma, *Nat. Rev. Mater.* **2019**, 4, 150.
- [7] P. Cappelletti, presented at *IEEE Int. Electron Devices Meeting (IEDM)*, San Francisco, December **2015**.
- [8] G. W. Burr, presented at *Non-volatile Memories Workshop*, San Diego, CA, March **2010**.
- [9] M. Wuttig, H. Bhaskaran, T. Taubner, *Nat. Photonics* **2017**, 11, 465.
- [10] Q. Wang, E. T. Rogers, B. Gholipour, C.-M. Wang, G. Yuan, J. Teng, N. I. Zheludev, *Nat. Photonics* **2016**, 10, 60.
- [11] G. W. Burr, R. M. Shelby, A. Sebastian, S. Kim, S. Kim, S. Sidler, K. Virwani, M. Ishii, P. Narayanan, A. Fumarola, *Adv. Phys.: X* **2017**, 2, 89.
- [12] B. Rajendran, A. Sebastian, M. Schmuker, N. Srinivasa, E. Eleftheriou, *IEEE Signal Process. Mag.* **2019**, 36, 97.
- [13] D. Loke, T. Lee, W. Wang, L. Shi, R. Zhao, Y. Yeo, T. Chong, S. Elliott, *Science* **2012**, 336, 1566.
- [14] G. Bruns, P. Merkelbach, C. Schlockermann, M. Salinga, M. Wuttig, T. Happ, J. Philipp, M. Kund, *Appl. Phys. Lett.* **2009**, 95, 043108.
- [15] F. Rao, K. Ding, Y. Zhou, Y. Zheng, M. Xia, S. Lv, Z. Song, S. Feng, I. Ronneberger, R. Mazzarello, *Science* **2017**, 358, 1423.
- [16] F. Xiong, A. D. Liao, D. Estrada, E. Pop, *Science* **2011**, 332, 568.
- [17] J. Y. Raty, M. Schumacher, P. Golub, V. L. Deringer, C. Gatti, M. Wuttig, *Adv. Mater.* **2019**, 31, 1806280.
- [18] Y. Cheng, O. Cojocar-Mirédin, J. Keutgen, Y. Yu, M. Küpers, M. Schumacher, P. Golub, J. Y. Raty, R. Dronskowski, M. Wuttig, *Adv. Mater.* **2019**, 31, 1904316.
- [19] M. Wuttig, V. L. Deringer, X. Gonze, C. Bichara, J. Y. Raty, *Adv. Mater.* **2018**, 30, 1803777.
- [20] M. Zhu, O. Cojocar-Mirédin, A. M. Mio, J. Keutgen, M. Kupers, Y. Yu, J. Y. Cho, R. Dronskowski, M. Wuttig, *Adv. Mater.* **2018**, 30, 1706735.
- [21] L. Guarneri, S. Jakobs, A. von Hoegen, S. Maier, M. Xu, M. Zhu, S. Wahl, C. Teichrib, Y. Zhou, O. Cojocar-Mirédin, M. Raghuvanshi, C. F. Schon, M. Drogeler, C. Stampfer, R. Lobo, A. Piarristeguy, A. Pradel, J. Y. Raty, M. Wuttig, *Adv. Mater.* **2021**, 33, 2102356.
- [22] S. Maier, S. Steinberg, Y. Cheng, C. F. Schon, M. Schumacher, R. Mazzarello, P. Golub, R. Nelson, O. Cojocar-Mirédin, J. Y. Raty, M. Wuttig, *Adv. Mater.* **2020**, 32, 2005533.
- [23] J. Y. Raty, W. Zhang, J. Luckas, C. Chen, R. Mazzarello, C. Bichara, M. Wuttig, *Nat. Commun.* **2015**, 6, 7467.

- [24] B. Huang, J. Robertson, *Phys. Rev. B* **2010**, *81*, 081204.
- [25] C. Persch, M. J. Müller, A. Yadav, J. Pries, N. Honné, P. Kerres, S. Wei, H. Tanaka, P. Fantini, E. Varesi, *Nat. Commun.* **2021**, *12*, 4978.
- [26] S. Buller, C. Koch, W. Bensch, P. Zalden, R. Sittner, S. Kremers, M. Wuttig, U. Schürmann, L. Kienle, T. Leichtweiß, *Chem. Mater.* **2012**, *24*, 3582.
- [27] Y. Zhang, J. B. Chou, J. Li, H. Li, Q. Du, A. Yadav, S. Zhou, M. Y. Shalaginov, Z. Fang, H. Zhong, *Nat. Commun.* **2019**, *10*, 4279.
- [28] W. Dong, H. Liu, J. K. Behera, L. Lu, R. J. Ng, K. V. Sreekanth, X. Zhou, J. K. Yang, R. E. Simpson, *Adv. Funct. Mater.* **2019**, *29*, 1806181.
- [29] M. Delaney, I. Zeimpekis, D. Lawson, D. W. Hewak, O. L. Muskens, *Adv. Funct. Mater.* **2020**, *30*, 2002447.
- [30] L. Zhang, Y. Li, C. Li, Q. Chen, Z. Zhen, X. Jiang, M. Zhong, F. Zhang, H. Zhu, *ACS Nano* **2017**, *11*, 12753.
- [31] U. A. Shah, S. Chen, G. M. G. Khalaf, Z. Jin, H. Song, *Adv. Funct. Mater.* **2021**, *31*, 2100265.
- [32] W. H. Zachariasen, *J. Am. Chem. Soc.* **1932**, *54*, 3841.
- [33] M. Putero, M.-V. Coulet, C. Muller, G. Cohen, M. Hopstaken, C. Baehtz, S. Raoux, *Appl. Phys. Lett.* **2014**, *105*, 181910.
- [34] K. Shportko, S. Kremers, M. Woda, D. Lencer, J. Robertson, M. Wuttig, *Nat. Mater.* **2008**, *7*, 653.
- [35] J.-Y. Raty, M. Wuttig, *J. Phys. D: Appl. Phys.* **2020**, *53*, 234002.
- [36] M. Lankhorst, *J. Non-Cryst. Solids* **2002**, *297*, 210.
- [37] A. Velea, *J. Optoelectron. Adv. Mater.* **2009**, *11*, 1983.
- [38] N. Amini, J. Pries, Y. Cheng, C. Persch, M. Wuttig, M. Stolpe, S. Wei, *Mater. Sci. Semicond. Process.* **2021**, *135*, 106094.
- [39] J. Pries, S. Wei, M. Wuttig, P. Lucas, *Adv. Mater.* **2019**, *31*, 1900784.